THE JOURNAL OF BIOLOGICAL CHEMISTRY VOL. 286, NO. 12, pp. 10803–10813, March 25, 2011

AaCAT1 of the Yellow Fever Mosquito, *Aedes aegypti*

*A NOVEL HISTIDINE-SPECIFIC AMINO ACID TRANSPORTER FROM THE SLC7 FAMILY**

Received for publication, August 27, 2010, and in revised form, January 15, 2011 Published, JBC Papers in Press, January 24, 2011, DOI 10.1074/jbc.M110.179739

Immo A. Hansen[‡1,2], Dmitri Y. Boudko[§1], Shin-Hong Shiao[¶], Dmitri A. Voronov[§], Ella A. Meleshkevitch[§], Lisa L. Drake[‡], Sarah E. Aguirre[‡], Jeffrey M. Fox[§], Geoffrey M. Attardo[‖], and Alexander S. Raikhel[**]

From the [‡]Department of Biology and Institute of Applied Biosciences, New Mexico State University, Las Cruces, New Mexico 88003-8001, the [**]Department of Entomology, University of California, Riverside, California 92521, the [§]Department of Physiology and Biophysics, Chicago Medical School, Rosalind Franklin University, North Chicago, Illinois 60064, the [¶]Department of Parasitology, National Taiwan University, Taipei 106, Taiwan, and the [‖]Yale School of Public Health, Yale University, New Haven, Connecticut 06520-8034

Insect yolk protein precursor gene expression is regulated by nutritional and endocrine signals. A surge of amino acids in the hemolymph of blood-fed female mosquitoes activates a nutrient signaling system in the fat bodies, which subsequently derepresses yolk protein precursor genes and makes them responsive to activation by steroid hormones. Orphan transporters of the SLC7 family were identified as essential upstream components of the nutrient signaling system in the fat body of fruit flies and the yellow fever mosquito, *Aedes aegypti.* However, the transport function of these proteins was unknown. We report expression and functional characterization of *AaCAT1*, cloned from the fat body of *A. aegypti*. Expression of *AaCAT1* transcript and protein undergoes dynamic changes during postembryonic development of the mosquito. Transcript expression was especially high in the third and fourth larval stages; however, the AaCAT1 protein was detected only in pupa and adult stages. Functional expression and analysis of *AaCAT1* in *Xenopus* oocytes revealed that it acts as a sodium-independent cationic amino acid transporter, with unique selectivity to L-histidine at neutral pH ($K_{0.5}^{\text{L-His}}$ = 0.34 ± 0.07 mM, pH 7.2). Acidification to pH 6.2 dramatically increases AaCAT1-specific His^+-induced current. RNAi-mediated silencing of *AaCAT1* reduces egg yield of subsequent ovipositions. Our data show that AaCAT1 has notable differences in its transport mechanism when compared with related mammalian cationic amino acid transporters. It may execute histidine-specific transport and signaling in mosquito tissues.

Mosquito-transmitted diseases like malaria and dengue fever are a global problem affecting hundreds of millions of people every year. Anautogenous mosquito females require vertebrate blood for reproduction, and it is the vector-host interaction during blood feeding that makes mosquitoes effective vectors for multiple infectious diseases. Blood is the sole source of amino acids (AAs)[3] in adult females, with the exception of stores acquired during the larval phase. Blood meal-derived AAs deliver energy and the essential building blocks for synthesis of yolk protein precursor (YPP) proteins that are deposited into developing eggs by the mother to provide nutrients necessary for embryonic development (1).

During mosquito vitellogenesis, YPP gene expression is activated exclusively in the mosquito fat body, the insect analog of the vertebrate liver (2, 3). Blood meal-derived AAs stimulate YPP genes via the target of rapamycin (TOR) signal transduction pathway (4, 5). Several AAs are essential for the activation of YPP genes in the fat body. This group includes the three cationic AAs, arginine, histidine, and lysine. Treatment of fat bodies with amino acid uptake inhibitors ouabain and bafilomycin resulted in inhibition of the amino acid-induced YPP gene expression, proving that facilitated transport is involved in the AA signaling mechanism (6). However, the exact nature of the transmembrane signaling and transporting events that cause fat body activation in mosquitoes is unknown.

In previous work, we cloned two putative orphan AA transporters that belong to the cationic amino acid transporter (CAT) subfamily of the SLC7 (solute carrier family 7) (7) from the fat body of *Aedes aegypti* females, *AaCAT1* and *AaCAT2*. AaCAT1, originally named *slif* (*A. aegypti slimfast*), was renamed after more sequence data became available (see below). RNAi-mediated knockdown of both transporters resulted in a strong decrease in the transcriptional response of YPP genes to amino acid stimulation similar to that observed during TOR inhibition (6). These results suggest that these two SLC-7 transporters are part of the TOR-signaling cascade, upstream of the TOR kinase.

In the fruit fly *Drosophila melanogaster*, three types of secondary transporters from the SLC7 and SLC36 families act as regulators of cell growth via TOR signaling. One of them, *Drosophila* SLIF, is part of the larval fat body nutrient sensor mechanism. It genetically interacts with the TOR signaling pathway in the fat body and mediates the repression of phosphatidylinositol 3-kinase signaling in peripheral tissues by an undefined endocrine regulator (8). Hennig *et al.* (9) have found that TOR signaling stimulates general endocytotic uptake of a hexamerin storage protein, whereas it inhibits the endocytotic uptake and

* This work was supported, in whole or in part, by National Institutes of Health (NIH) NIAID Grant 5R37AI024716 (to A. S. R.), NIH, NIGMS, Grant 1SC2GM092300-01 (to I. A. H.), and NIH, NIAID, Grant R01 AI-030464 (to D. Y. B.).

[1] Both authors contributed equally to this work.

[2] To whom correspondence should be addressed. Tel.: 575-646-7719; Fax: 575-646-5665; E-mail: immoh@nmsu.edu.

[3] The abbreviations used are: AA, amino acid; YPP, yolk protein precursor; TOR, target of rapamycin; CAT, cationic amino acid transporter; HAT, heterodimeric transporter; TMD, transmembrane domain; DA, dopamine; IV, current-voltage dependence.

degradation of SLIF protein in the larval fat body, resulting in a positive effect on bulk endocytosis and a negative effect on endocytotic degradation. Fat body SLIF is associated with the regulation of lipid accumulation in oenocytes of *Drosophila* larvae (10).

An AA transporter of the SLC36 family in *Drosophila*, pathetic (PATH), also regulates TOR activity in different tissues. This transporter has a very low transport capacity and an exceptionally high substrate affinity, and it was suggested that PATH may control growth by functioning as an AA sensor or transceptor (11). A third AA transporter, MINIDISCS, a light chain subunit of the heterodimeric transporter (HAT)-SLC7 subfamily is essential for amino acid-activated endocrine regulation of fly growth by the fat body (12).

Here we report the molecular and functional characterization of *AaCAT1* from the yellow fever mosquito, *A. aegypti*. The *AaCAT1* transcript and protein expression profiles were determined during mosquito postembryonic development, and functional electrochemical characterization was conducted using heterologous expression of *AaCAT1* transcript in *Xenopus laevis* oocytes with subsequent electrophysiological recording of amino acid-induced currents and quantitative radiolabeled amino acid uptake assays.

EXPERIMENTAL PROCEDURES

Mosquito Rearing—The *A. aegypti* mosquito strain UGAL/Rockefeller was maintained in laboratory culture as has been previously described by Hays and Raikhel (13). The strain was reared at a temperature of 28 °C with 80% humidity and a photoperiod of 14 h light and 10 h dark. Larvae were fed on a diet of ground rat food, yeast, and albumin (1:1:1, w/w/w).

Bioinformatics—NCBI protein databases were screened for AaCAT1 homologs using BLASTp (14). Selected sequences from different insect species ($e < 10^{-3}$ cut-off) were used for multiple protein sequence alignment with the amino acid translation of *AaCAT1*. An iterative alignment was performed using the MEGA (15) implementation of the MUSCLE (16) algorithm followed by final manual correction with consideration for the ApcT three-dimensional structure (17) and predicted two-dimensional structures of other SLC7 members. The evolutionary history was analyzed using the neighbor-joining, minimum evolution, maximum parsimony, and Bayesian methods that produced similar tree topologies. The neighbor-joining tree was selected as a more common representation of the evolutionary history of transport proteins. The tree was visualized using FigTree 1.3.1 software (A. Rambaut). It was drawn with estimated branch lengths used to infer the tree relative to a 3.7 billion-year-long scale from the root.

Expression Studies—Total RNA was obtained from different larval stages, pupae, and adult females with TRIzol® solution (Invitrogen) (19). Tissue-specific RNAs were isolated after dissection of samples from 30 individual mosquitoes, including previtellogenic females 72 h after eclosion and female mosquitoes 24 h post-blood meal. Transcript was quantified using reverse transcription-PCR and real-time quantitative PCR using iQ Supermix (Bio-Rad). Primers and probes were as follows (all Taqman probes used the Black Hole Quencher and were synthesized by Qiagen (Valencia, CA)): AaCAT1 forward, 5′-ctg gtt ggc ttc gtg at-3′; AaCAT1 reverse, 5′-ctc tag ttg act ttc cga c-3′; AaCAT1 probe, 5′-6-carboxyfluorescein (FAM)-cat tcg gtt ctt ggc tcc-Black Hole Quencher 1-3′.

RNAi Knockdown Experiments—Generation of double-stranded RNAs (dsRNA) was performed as described earlier (6) using the MEGAscripts T7 kit (Ambion, Austin, TX). Approximately 500 ng of dsRNA in 268 nl of pyrogen-free H_2O was injected into the thorax of CO_2-anesthetized female mosquitoes 3 days after adult emergence. The injected mosquitoes were then allowed to recover for 3 days. Knockdown effectiveness was confirmed with RT-PCR.

Antibody Production—Antisera were generated against an *AaCAT1* cDNA fragment representing amino acids 381–591 of the AaCAT1 protein. The cDNA was cloned into pRSET-A, and recombinant protein was expressed in *E. coli* BL21 cells (Invitrogen) following the manufacturer's protocol. Antibody production was conducted by Cocalico Biologicals Inc. (Reamstown, PA) facilities. Affinity-purified antibodies (NAb™ Protein A/G Spin Kit, Thermo, Waltham, MA) were used for Western blot analysis.

Construction of an AaCAT1 Expression Vector—Cloning procedures were similar to those previously used for heterologous expression and characterization of mosquito transporters (20). The full-length cDNA of *AaCAT1* was amplified using the following primers with attached Sfi1 restriction site sequences at the 5′ and 3′ ends: 5′-tcg gcc ccg cgg gcc ATG GAC AAA TTC TTC AAG GCC CTC TGC CGC AAA AAA CCA AAC GA and 3′-gtg gcc cgc ggg gcc CTA CGC CTT TTC GAG TCC TAC CAT GCA GAA CGG ATT CTC TAG T. The PCR fragment was digested with Sfi1 and subsequently cloned into the *Xenopus* expression vector pXOON.

Heterologous Expression—cRNA for oocyte injections was obtained by *in vitro* transcription of XbaI-linearized pXOON-*AaCAT1* plasmids using the mMessage-mMachine® (Ambion Inc., Carlsbad, CA). The integrity and quantity of the transcript was confirmed by agarose gel electrophoresis. Surgically isolated and collagenase-treated stage V-VI *X. laevis* oocytes (Nasco, Fort Atkinson, WI) were injected with ~40 ng of *AaCAT1* cRNA and incubated for 2–6 days at 17 °C in sterile 98 mM Na^+ oocyte buffer that was supplemented with 2.5 mmol/liter sodium pyruvate, 100 units/ml penicillin, 100 mg/ml streptomycin, and 5% horse serum and adjusted to pH 7.2.

Electrophysiological Characterization—4–6 days postinjection oocytes were used in all experiments. Individual oocytes were placed in a ~50-μl volume constant flow perfusion chamber connected to a custom 20-valve perfusion system. The perfusion rate was adjusted to ~20 μl/s, which corresponds to ~3 s for complete solution replacement. Transmembrane currents were recorded using a two-electrode voltage clamp system (OC-725C, Warner Instruments, LLC, Hamden, CT). AA-induced currents and episodic stimulation invents were digitized and acquired on a PC using paired analog digital converters, MiniDIGI, for continuous recording of current voltage signals at 500 data points/s and DigiData 1322A for snapshot recording of the current-voltage relationship (4-s rump from −80 to +70 mV at −50 mV holding potential, 1000 points/s) using Axoscope and pCLAMP software modules, respectively (Molecular Devices, Sunnyvale, CA). The composition of solutions for elec-

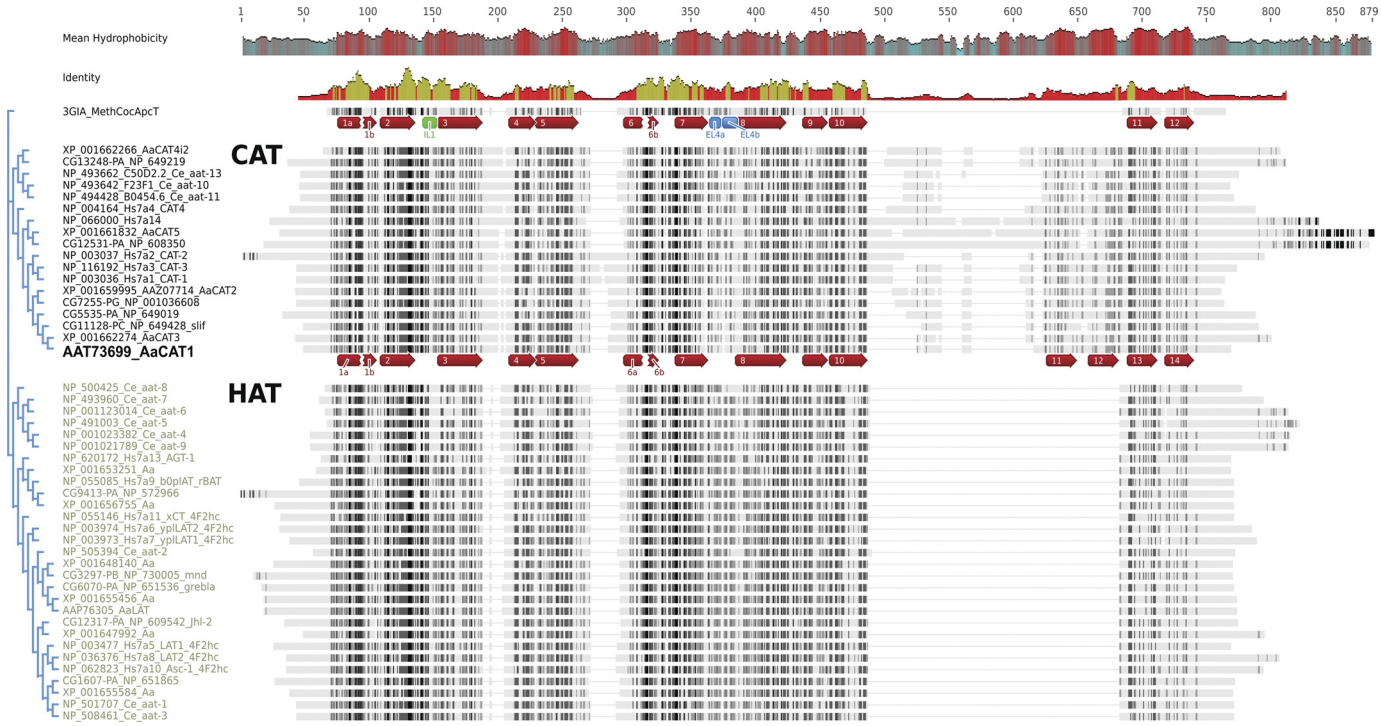

FIGURE 1. **Protein sequence/two-dimensional structure alignment of *A. aegypti CAT1* with selected species-specific groups of the SLC7 family.** A homologous protein structure (Protein Data Bank accession number 3GIA, ApcT from a thermophilic archaeon, *Methanocaldococcus jannaschii*) was used in the accurate protein sequence and structure alignments of SLC7 families groups from fruit fly *D. melanogaster*, mosquito *A. aegypti*, nematode *Caenorabditis elegans*, and mammalian representative *Homo sapiens*. Sequences are sorted according to a draft phylogenetic tree shown on the *left side* of the alignment. A gradually darker pattern represents higher sequence similarity. The alignment of the last two TMDs was manually improved, resulting in better pairwise sequence identity. The *red arrows* and *green* and *blue blocks*, respectively, depict conserved transmembrane domains and intracellular and extracellular helices, shown for ApcT and AaCAT1.

trophysiological recording and uptake assays was described previously (20). For the analysis of AaCAT1 pH dependence, the base solution with 98 mM NaCl was adjusted to pH 6.2, 7.2, 8.2, and 9.2 using 2 N solutions of HCl or NaOH. Signals were filtered and analyzed using ClampFit 10.2 (Molecular Devices) and converted to report graphs as described previously (21).

Isotope-labeled Amino Acid Uptake—The uptake was performed according to a previously published protocol (22), with some modifications. Specifically, groups of five *AaCAT1* cRNA- or water-injected or uninjected oocytes were incubated in 0.2 ml of 98 mM Na^+ buffer with adjusted pH and specified amounts of radiolabeled and unlabeled amino acids, as shown for specific experiments under "Results." Isotope-labeled amino acids (L-[*ring*-2,5-^{3}H]histidine, specific activity 55.4 Ci/mmol; L-[^{14}C(U)]arginine, specific activity 0.31; L-[1-^{14}C]methionine, specific activity 0.054; L-[*ring*-2,4-^{3}H]phenylalanine, specific activity 23; L-[2,3-^{3}H]alanine, specific activity 49.4; and L-[4,5-^{3}H]lysine) were purchased from Moravek Biochemicals, Inc. The uptake was terminated after the time intervals by washing oocytes with an excess volume of ice-cold 98 mM Na^+ buffer four times. Individual oocytes were dissolved in scintillation tubes with 0.2 ml of 10% SDS. 2 ml of scintillation fluid was added. The radioactivity was determined using a Beckman-Coulter LS 6500 scintillation counter.

Statistical Methods—Values depicted for the presentation of electrophysiological and uptake data represent the mean ± S.D. or S.E. of at least three independent data points from at least three different oocytes. Excel (Microsoft Inc.) and SigmaPlot 11 (SSI, San Jose, CA) software was used to analyze statistical data and generate final graphs. The electrical current amplitudes were normalized relative to a maximum current in their individual oocyte data set. Kinetic profiles and constants were determined by fitting normalized data sets of several statistical samples with a three-parameter Michaelis-Menten and Hill equation using the Sigma Plot regression analysis tool. Average accumulation of specific radiolabeled substrates in control oocytes was subtracted before statistical analysis. From the five oocyte samples, the highest and smallest values were omitted, and the remaining three were used for calculations.

RESULTS

Phylogenetic Analysis—Fig. 1 represents a comprehensive homology/hydrophobicity pattern and secondary structure alignment of *A. aegypti* AaCAT1 with SLC7 members from selected invertebrate and mammalian model organisms. All SLC7 transporters share a secondary structure with conserved transmembrane domains (TMDs). *A. aegypti* AaCAT1 is a member of the CAT subfamily (CAT-SLC7; Fig. 2), all of which have 14 putative TMDs. Automatic approaches produced an ambiguous alignment of the last few TMDs of CAT and HAT transporters. However, after manual improvement, we found enhanced pairwise sequence identities of TMDs 11 and 12 in HATs with TMDs 13 and 14 in CATs when compared with CAT TMDs 11 and 12. This suggests a duplication of the last two TMDs of an ancestral 12-TMD protein as the origin of the 14-TMD CAT structure. This duplication resulted in the inser-

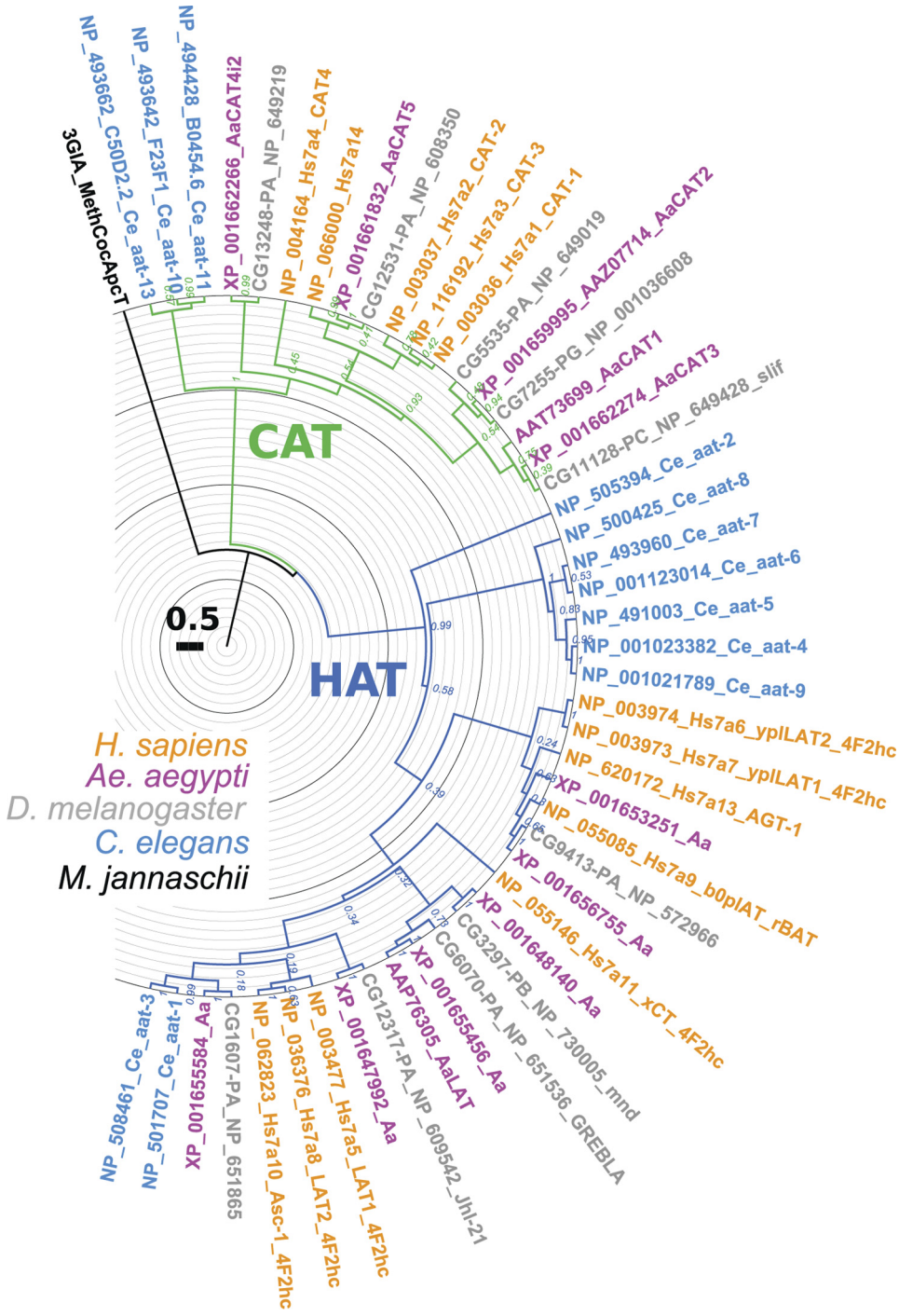

FIGURE 2. **Phylogenetic tree of AaCAT1 and selected SLC7 transporters.** The evolutionary history was inferred using the neighbor-joining method (34). The optimal tree with the sum of branch length = 25.84 is shown. The percentage of bootstrap test (10,000 replicates) is shown next to the branches (35). The tree is drawn using FigTree software to an approximately 3.7 billion-year-long scale with relative branch lengths used to infer the tree. The evolutionary distances were computed using the Poisson correction method (18) and are in units of the number of amino acid substitutions per site. The rate variation among sites was modeled with a γ distribution (shape parameter = 1). The analysis involved 48 amino acid sequences. All positions containing fewer than 95% alignment gaps and missing data were eliminated, leading to 445 positions in the final data set. Evolutionary analyses were conducted in MEGA4 (15).

tion of two additional TMDs between TMD 10 and 11. It occurred ~2.6 billion years ago, probably soon after the bifurcation of eukaryotic and archaean branches (Fig. 2). However, the apparent CAT expansion represents more recent events ~1 billion years ago that may coincide with expansion of metazoan organisms. In contrast, the HAT expansion ~1.6 billion years ago may coincide with the expansion of eukaryotic forms.

AaCAT1 is closely related to another mosquito transporter, AaCAT3, which, together with *Drosophila* Slif, forms the most recent ~100 million-year-old cluster that is separated from the mammalian and nematode CATs with greater evolutionary distances (Fig. 2, *Ce_aat cluster*). Two additional mosquito CATs, AaCAT4 and AaCAT5, are present in the basal part of the CAT-SLC7 branch. AaCAT5 and *Drosophila* CG12531 share a

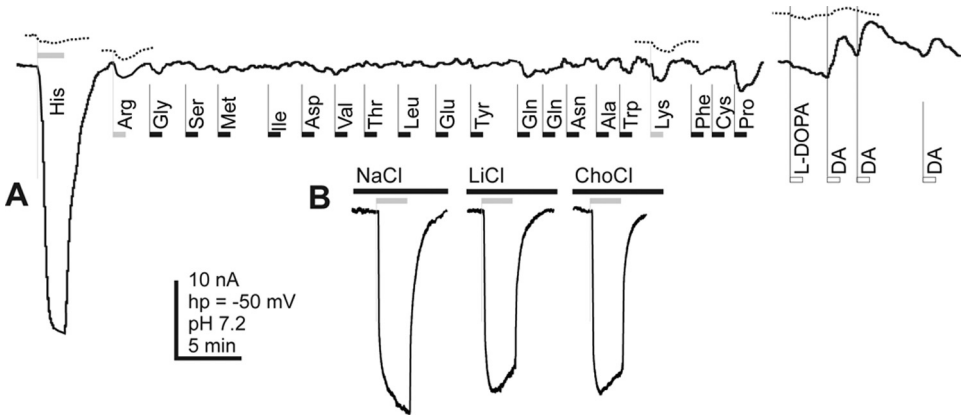

FIGURE 3. **Functional expression and ion dependence of *AaCAT1* in *Xenopus* eggs.** Oocytes were used 4–5 days after injection of iCAT1 mRNA. Control oocytes were injected with 40 nl of deionized water. *A*, current traces recorded during application of different substrates on a representative *AaCAT1*-expressing *Xenopus laevis* oocyte (*solid line*) and control uninjected oocyte (*dotted line*) are shown for selected canonical L-amino acids, DA, and dopamine precursor (*L-DOPA*)). All substrates were applied at constant flow rates switching between 98 mM Na^+ (pH 7.2) solutions and an identical solution with the addition of 2 mM indicated substrates at −50 mV holding transmembrane voltage (two-electrode voltage clamp mode). *B*, 2 mM His-induced currents in an *AaCAT1*-expressing oocyte in 98 mM NaCl, 100 mM LiCl, and 100 mM choline-Cl solutions, respectively.

cluster with mammalian CATs, three of which, CAT1, -2, and -3, have been characterized as transporters of cationic L-lysine, L-arginine, and L-ornithine in different parts of the mammalian alimentary canal (7).

Functional Expression and Characterization of AaCAT1—To determine substrate specificity and electrochemical properties, *AaCAT1* was expressed in *X. laevis* oocytes and characterized using electrophysiological and radiolabeled amino acid uptake assays. *AaCAT1* expression slightly reduces rest membrane voltage (V_m) and increases leak current (I_m) in oocytes ($V_m = 27 \pm 7.6$; $I_m = 78 \pm 36$ nA at −50 mV holding voltage, pH 7.2; $n = 7$) compared with uninjected control oocytes ($V_m = 35 \pm 10.6$ and $I_m = 17 \pm 10$ nA; $n = 5$; pH 7.2). Minor endogenous amino acid-induced currents in *Xenopus* oocytes have been reported previously (23). Similarly, canonical amino acids as well as related enantiomers in concentrations up to 5 mM (2.5 mM for L-Tyr) induced no or minor transmembrane currents in control oocytes at neutral pH 7.2 ($I_m \leq 6 \pm 3.2$ nA; $n > 3$ for each data point; Fig. 3*A*) (data not shown). No significant amino acid-induced currents were observed in *AaCAT1*-injected oocytes for the majority of tested amino acids applied at pH 7.2, including cationic L-Lys and L-Arg. In contrast, application of L-His induced robust inward currents (59.3 ± 26.2 nA for 2 mM L-His; Fig. 3*A*). Such current was absent in control oocytes (Fig. 3 A, *dotted lines*). The His-induced currents were reduced by a fraction of 7.2 ± 4.6% ($n = 10$) upon substitution of Na^+ for K^+ or $choline^+$ cations (Fig. 3*B*), suggesting that the observed current is largely Na^+-independent. This also may suggest that the recorded inward current is generated by charge translocation upon uptake of His^+ cations. However, His has a complex dissociation behavior in the subneutral region (pK_a His = 1.7, 6.02, and 9.08). At pH 7.6, the net charge of His is zero, although the molecule contains two almost completely ionized groups. At pH 7.2, only 6.1% of the imidazole groups are protonated, and His carries a positive charge, whereas 92.7% remains neutral.

To expand the analysis of AaCAT1, we tested selected products of the amino acid metabolism, including different components of neurotransmitter synthesis cascades: γ-aminobutyric acid, serotonin, 5-hydroxytryptophan, dopamine (DA), dopamine precursor, and metabolic cationic amino acids. In the selected set, only dopamine produces a notable effect (Fig. 3*A*). Specifically, the application of 2 mM DA induced outward current. Control oocytes were insensitive to DA at pH 7.2 (Fig. 3*A*, *dotted trace*), suggesting that the above effect may be due to the reduction of AaCAT1-coupled cationic leak current rather than absorption of DA^+ (pK_a DA = 8.9).

Extracellular acidification to pH 6.2 dramatically increases His-induced currents (~4.5 times), but minute changes were observed in AaCAT1-injected oocytes in response to L-Arg and L-Lys (Fig. 4*A*). Minor increases of cationic AA-induced currents were observed in control oocytes upon acidification from pH 7.2 to pH 6.2 (Fig. 4, *A* (*dotted trace*) and *B*). The pH dependence of AaCAT1 may reflect the surge of effective concentration of His^+, estimated to be 39.8% at pH 6.2, which is consistent with CAT-characteristic transport of cationic substrates (6). An alternative possibility is that His currents are induced by coupled translocation of neutral His and H^+. Upon acidification from pH 7.2 to pH 6.2, the effective concentration of neutral His decreases only 35% (about one-third), whereas the proton motive forces increase 10 times. Such a mechanism would be inactivated or reversed upon exposure of oocytes with a neutral intracellular pH or alkalinization (24). We tested this possibility and found that the His-induced current remains cationic-inward at pH 8.2. Therefore, a proton-neutral His-coupled mechanism appears unlikely. At pH 9.2, the cationic amino acid-induced currents were inversed, which correlates with cationic outward or anionic inward fluxes (Fig. 4, *A* (*lower trace*) and *B*). Such currents may reflect an absorption of His^- (~56% at this pH 9.2) or secretion of His^+ ions. A similar inversion of His-induced currents at high pH was previously described in the study of rBAT, a heavy-chain subunit associated with mammalian HAT-SLC7 members (25). Surprisingly, at pH 8.2, AaCAT1 oocytes generate large and comparable responses to L-Arg and L-Lys. We performed an additional set of control experiments using sam-

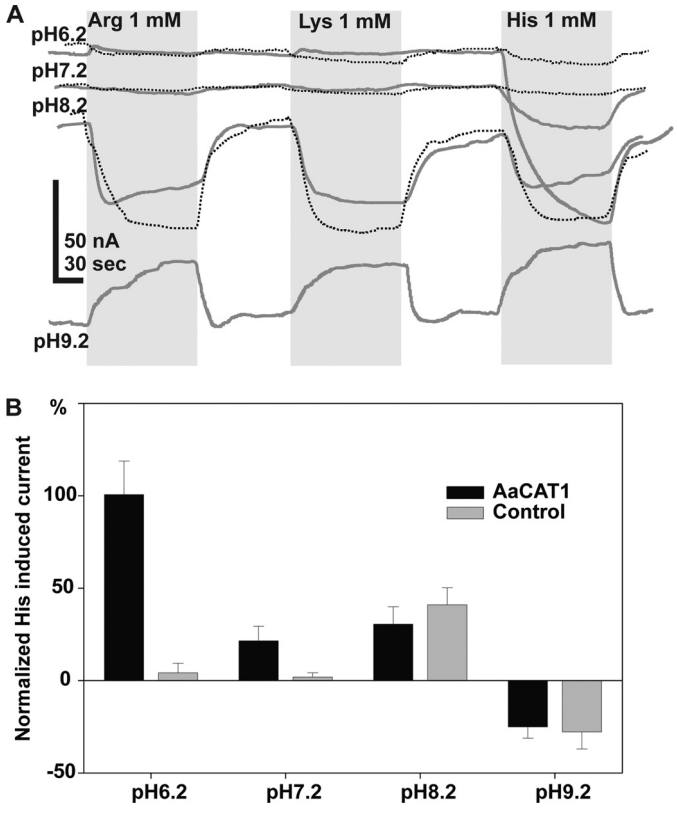

FIGURE 4. **pH-dependent modulation of cationic amino acid-induced currents in *AaCAT1*-injected and control oocytes.** Experimental and control oocytes were treated in identical conditions and recorded on the 5th day after injection of the experimental set. *A*, current trace during application of 1 mM L-Arg, L-Lys, and L-His at pH 6.2, 7.2, and 8.2 in *AaCAT1*-injected (*solid line*) and uninjected control oocytes (*dotted lines*) are shown. *B*, quantification of 1 mM L-His-induced currents at different pH values (*bars* are the normalized mean of current amplitudes ± S.D. (*error bars*) for $n > 3$ oocytes in each data point). The oocytes used were taken from different egg batches by three individual *Xenopus* females.

ples of uninjected oocytes from four different frogs and found that the L-His-, L-Arg-, and L-Lys-induced currents at pH 8.2 are an endogenous property of *Xenopus* oocytes. At pH 8.2, the control oocytes demonstrate the presence of a previously unnoticed endogenous broad spectra cationic amino acid transport system (Figs. 4 and 5) (data not shown). Fortunately, endogenous currents did not interfere with the recording of AaCAT1-coupled currents at neutral and acidic conditions. High pH data is not critical in unraveling the *in vivo* function of AaCAT1.

As mentioned above, small responses ($<7 \pm 3.4$ nA) to a variety of cationic amino acids were also recorded in control oocytes at pH 6.2 but not at pH 7.2 (see an example of the control oocyte recording in Fig. 5*A*). To differentiate AaCAT properties from this endogenous transport system, we performed a comprehensive high resolution analysis of the current-voltage dependence (IV) of AaCAT1 (Fig. 5*B*). Our analysis revealed that the L-His-induced currents have nonlinear characteristics. The apparent reversion potential of His-induced current was in the +20 to +50 mV region, which may represent the anticipated electrochemical equilibrium of L-His^+ cations at the oocyte membrane. Our analysis indicates that the AaCAT1 transport mechanism is stereospecific. In particular, it generates dramatically stronger currents in response to L-His compared with D-His (Fig. 5*B*).

His-induced currents were saturable with a half-maximum saturation constant $K_{0.5}^{\text{L-His}} = 0.34 \pm 0.07$ mM and an apparent Hill constant $\eta = 1.26 \pm 0.2$ (Fig. 6), suggesting a one-substrate molecule per translocation event stoichiometry. However, considering the possible selectivity of AaCAT1 to His^+ cations and the partial protonation of His at pH 7.2 (~6.1%), the estimated values are $E_{0.5}^{\text{L-His}^+} = 20.7 \pm 4$ μM and $K_{0.5}^{\text{L-His}} = 27.5 \pm 10.37$ μM. *AaCAT1* expression correlates with a notable increase of L-His uptake with a relatively stable uptake rate during the first 15 min of ~4 pmol/oocyte/min (Fig. 7*A*). The apparent leveling of the amino acid uptake may reflect a gradual increase of intracellular substrate concentration that reduces electrochemical motive forces for the amino acid absorption and equalizes an efflux/influx process.

In a substrate competition experiment, using unlabeled amino acids, application of L-His, L-Lys, and L-Arg as well as several neutral AA resulted in notably reduced uptake of radiolabeled L-His (Fig. 7*B*). However, no significant AaCAT1-mediated uptake was detected for tested radiolabeled L-Met and L-Arg (Fig. 7*C*).

AaCAT1 Expression Patterns during Adult Development—To investigate the mRNA and protein expression profiles of *A. aegypti AaCAT1* during different developmental stages, we used real-time PCR and Western blotting (Fig. 8*A*, *top*). *AaCAT1* transcript was most abundant during the third and fourth larval stages, the pupal stage, and early after eclosion. Transcript concentrations subsequently decayed as observed previously (6).

To test if AaCAT1 protein expression patterns are identical with mRNA expression patterns, we performed a Western blot analysis with samples from larvae, pupae, and adult females. Surprisingly, our analysis revealed that AaCAT1 protein is expressed in pupae and adults only (Fig. 8*A*, *bottom*). We did not find any AaCAT1 protein in the larval protein samples.

In order to study the expression of *AaCAT1* mRNA in adult tissues, we performed quantitative real-time PCR analysis of the distribution of *AaCAT1* mRNA in different organs and body parts of female mosquitoes, 72 h post-eclosion. We found highly elevated levels of *AaCAT1* mRNA in the thorax and to a lesser degree in Malpighian tubules. Expression levels were relatively low in all other samples we analyzed: head, fat body, midgut, and ovary (Fig. 8*B*). We analyzed the mRNA expression patterns in different tissues of the thorax and found elevated expression in muscle tissue (Fig. 8*C*). Data from microarray analysis showed that in whole mosquitoes after a blood meal, *AaCAT1* mRNA levels rise and peak around 12 h post-blood meal and fall back to normal levels afterward (26).

Effect of RNAi-mediated AaCAT1 Knockdown on Mosquito Fecundity and Life Span—To test whether the AaCAT1 protein expression is important for mosquito egg development, we performed RNAi-mediated knockdown. Female mosquitoes 72 h after emergence were injected with dsRNA against *AaCAT1* or with a control dsRNA (MAL). After a 3-day

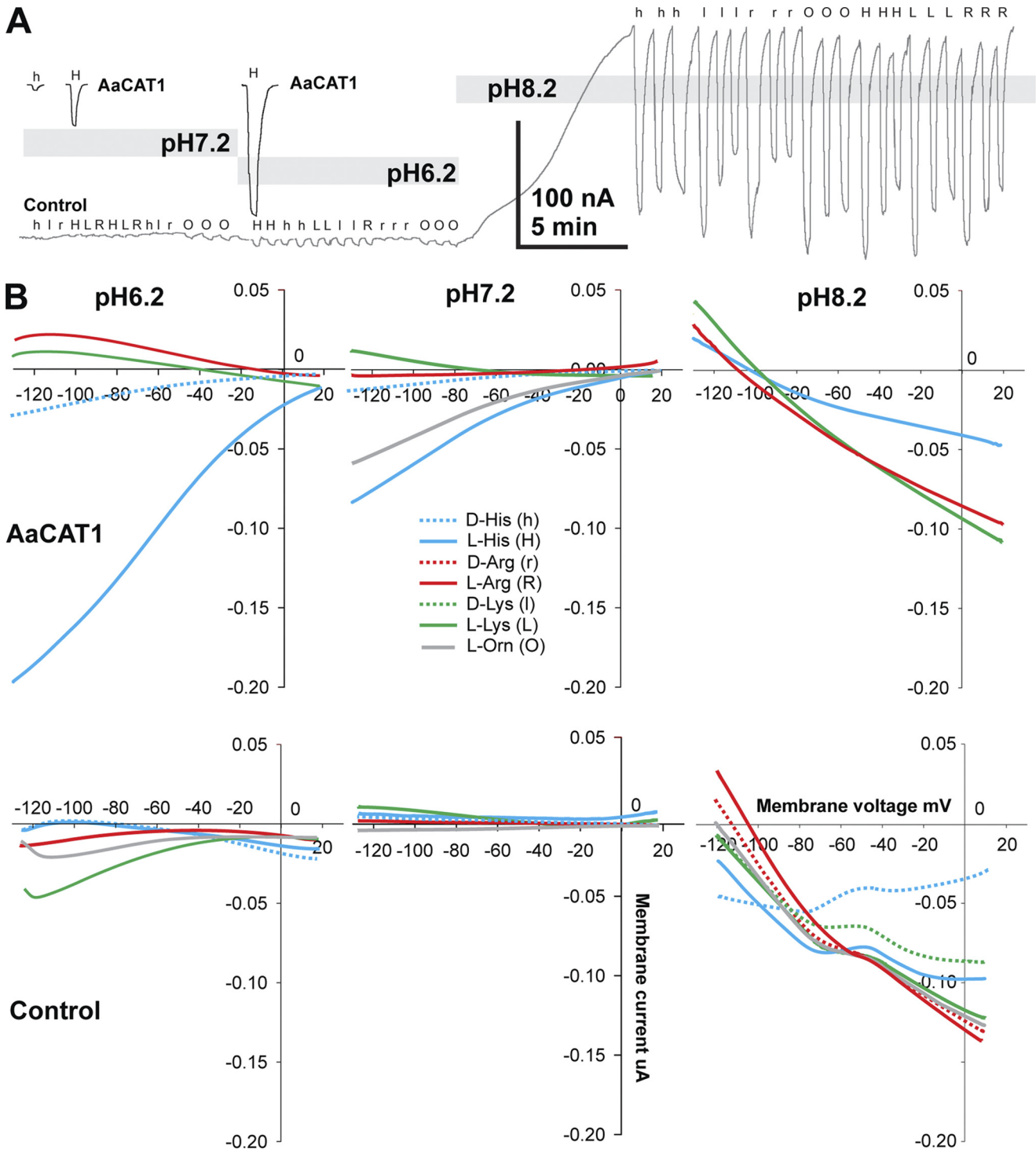

FIGURE 5. **Voltage- and pH-dependent modulation of cationic amino acid-induced currents in *AaCAT1* and control oocytes.** *A*, a representative continuous recording of transmembrane currents in a control (uninjected) oocyte (*gray line*) during changes of pH in the perfusion medium (*gray bars*) and episodic applications of specific amino acids. The application events are indicated using the *single-letter amino acid codes*, with *capital letters* for L-amino acids, *lowercase letters* for D-amino acids, and *O* for L-ornithine. All substrates were applied at 1 mM concentration after dilution in 98 mM Na^+ solution with specified pH values. The two-electrode voltage clamp mode with −50 mV holding voltage was used during all recordings. Signal was filtered using a digital 8-pole Bessel filter, and short high amplitude bursts of currents during rump stimulation were deleted from the recording. The *solid black line* shows selected fragments of a recording from an *AaCAT1*-injected oocyte at equivalent pH values. *B*, a collection of IV plots after application of selected basic amino acids. IVs for specific D- and L-amino acids are shown as dotted and *solid lines*, respectively, of *different colors* (*middle*). The *panels* summarize IVs from *AaCAT1*-expressing and uninjected oocytes (*AaCAT1* and *Control rows*) at three different pH values (*pH6.2*, *pH7.2*, and *pH8.2 columns*). Data were acquired using episodic rump stimuli before application of specified amino acids and before washing. IV was built by point-by-point subtraction of the first current trace recording from the second, which resulted in the specific amino acid-induced component of the current.

recovery, mosquitoes were given a blood meal. Only fully engorged mosquitoes were used in this experiment. After 3 days, egg deposition was triggered by allowing the mosquitoes access to a cotton ball soaked in water. Egg numbers were determined by a stereo microscope 24 h later. In three independent experiments, *AaCAT1*-injected mosquitoes

showed a significant reduction in the numbers of eggs they deposited (Fig. 9).

We also tested if knockdown of *AaCAT1* has an influence on mosquito life span. In three independent experiments, we found no significant effect of *AaCAT1* knockdown on mosquito life span (data not shown).

DISCUSSION

Reproductive success in anautogenous female mosquitoes depends on vitellogenesis, the rapid conversion of blood meal proteins into mosquito yolk proteins for deposition in developing eggs. Yolk proteins are used in embryonic and early postembryonic development of mosquitoes. The nutrient signaling and transport processes underlying vitellogenesis are only partly understood. Previous studies have shown that AaCAT1 and AaCAT2 are part of the fat body nutrient AA signaling system and necessary for the onset of vitellogenesis after a blood meal (6); however, the transport functions of these transporters in mosquitoes were unknown and impossible to predict because no closely related transporters were characterized at this time. The present study reveals the phylogenetic relationships, transport function, and expression patterns of *AaCAT1* and shows that it is essential for efficient mosquito egg development in the yellow fever mosquito, *A. aegypti*.

AaCAT1 is a member of the CAT subfamily of the SLC7 family of AA transporters, which has a characteristic 14-TMD structure that differentiates the CAT subfamily from the 12-TMD-containing members of the neighboring HAT subfamily (27). The results of our analysis (Fig. 1) suggest that CATs evolved upon duplication of the last two TMDs in an ancestral 12-TMD-containing HAT-like transporter. This duplication might have resulted in the loss of the functional requirement of these proteins for an auxiliary subunit, as seen in the HAT subfamily. Functional expression of HAT requires the association of a core SLC7 subunit with an auxiliary subunit from the SLC3 family, whereas such association is not required for functional expression of CAT proteins (7). Three of the five mammalian CAT-SLC7 transporters are characterized. All characterized mammalian CATs (SLC7A1 to -3, also called CAT1 to -3) resemble transporters from the y^+ transport system, which in general mediate transport of cationic AAs in plasma membrane of cells of different tissues (28). The characterized mammalian transporters predominantly transport Lys and Arg and act as exchangers or facilitators.

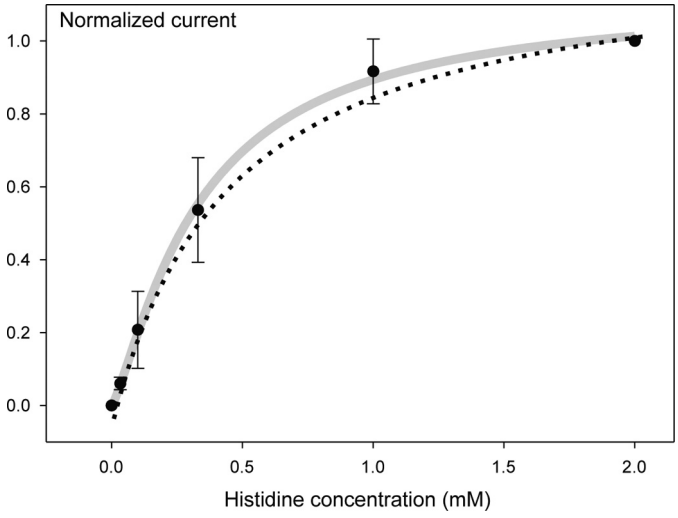

FIGURE 6. **Kinetic profile of L-His-induced currents in *AaCAT1*-injected oocytes.** L-His-mediated currents were saturable (means ± S.E.; $n \geq 3$ extrapolated with a Hill *solid gray line* (half-maximum saturation $E_{0.5}^{\text{L-His}^+} = 0.34 \pm 0.07$ mM; Hill constant $\eta = 1.26 \pm 0.2$; $n = 14$) and Michaelis-Menten *dotted line* functions ($K_{0.5}^{\text{L-His}} = 0.45 \pm 0.17$ mM; $n = 14$). The analysis was performed at pH 7.2. Considering possible selectivity of AaCAT1 to His^+ cation and partial protonation of His under this condition (6.1%), the estimated values will be $E_{0.5}^{\text{L-His}^+} = 20.7 \pm 4$ μM and $K_{0.5}^{\text{L-His}} = 27.5 \pm 10.37$ μM.

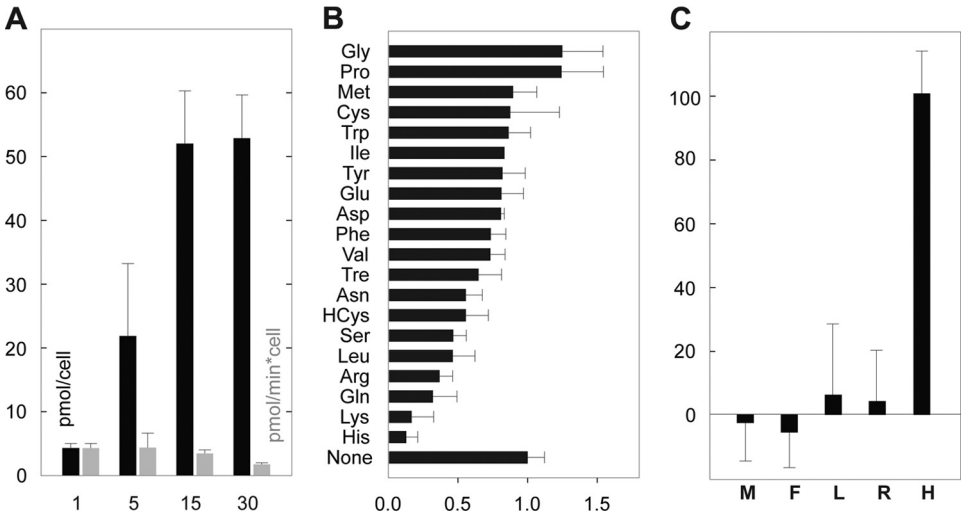

FIGURE 7. **AaCAT1-mediated uptake of isotope-labeled substrates in *Xenopus* oocytes.** *A*, a time course of His uptake in *AaCAT1*-injected and uninjected control oocytes. Shown are total amount (*black bars*) (pmol/oocyte) and ratio (*gray bars*) (pmol/oocyte/min) of L-histidine uptake measured after 1, 5, 15, and 30 min in individual *AaCAT1*-injected oocytes incubated in 98 mM Na^+ solution of 5 mM final concentration of L-His (1:100 L-[*ring*-2,5-^{3}H]His/unlabeled L-His; *bars* show mean ± S.D. (*error bars*) for $n \geq 4$ independent data points). After this experiment, 15 min was considered as the most appropriate linear uptake interval. *B*, a competitive amino acid-induced inhibition of radiolabeled histidine accumulation in the *AaCAT1*-expressing oocytes. The uptake of 1:100 stock radiolabeled L-His was measured in the presence of 5 mM concentration (except for 2.5 mM L-Tyr) of competing amino acids (*bars* represent mean ± S.D., $n \geq 3$ for each specified inhibitor). The average counts in control oocytes exposed to the identical uptake conditions were subtracted before statistical evaluation. *C*, relative uptake of selected amino acids after a 15-min incubation of *AaCAT1*-expressing oocytes in a 1:100 98 mM Na^+ solution of isotope-labeled amino acids. Nonspecific accumulation of radiolabeled substrates in uninjected oocytes was subtracted. All uptake experiments were performed at pH 7.2.

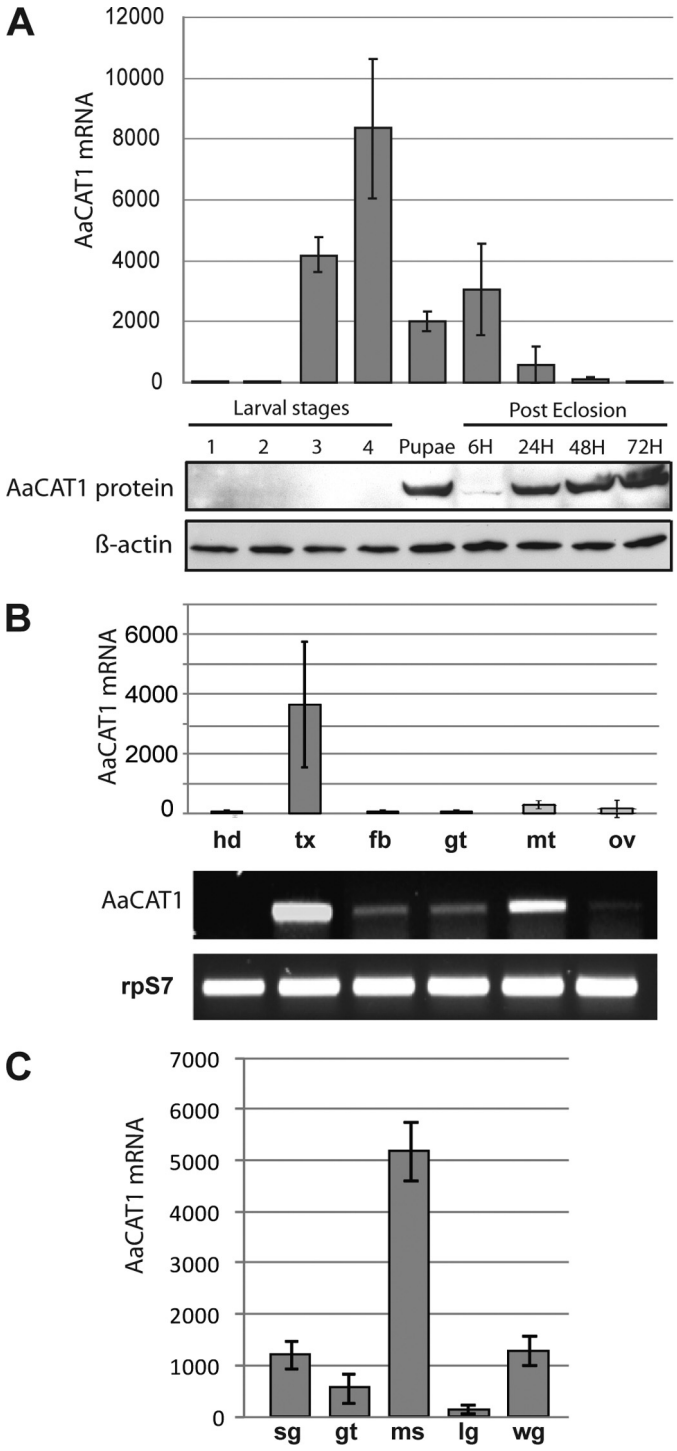

FIGURE 8. ***AaCAT1* is expressed in adult tissues and regulates reproduction.** *A*, AaCAT1 developmental expression patterns. *Top*, relative *AaCAT1* mRNA expression levels were determined via real-time PCR from samples isolated from total larvae, pupae, and adult mosquitoes. Data were normalized by real-time PCR analysis of ribosomal protein S7 mRNA levels in the cDNA samples. Values are means ± S.E. (*error bars*) of triplicate samples. *Bottom*, Western blot analysis of AaCAT1 protein. *B*, *AaCAT1* organ/body part expression patterns. *Top*, relative *AaCAT1* mRNA expression levels from different organs/tissues of female mosquitoes. Values are means ± S.E. of triplicate samples. *Bottom*, RT-PCR results; *hd*, head; *tx*, thorax; *fb*, fat body; *gt*, midgut; *mt*, Malpighian tubules; *ov*, ovaries. *C*, *AaCAT1* thoracic tissue expression patterns. Shown are relative *AaCAT1* mRNA expression patterns from different tissues isolated from the thorax. *sg*, salivary glands; *gt*, gut; *ms*, flight muscle; *lg*, legs; *wg*, wings.

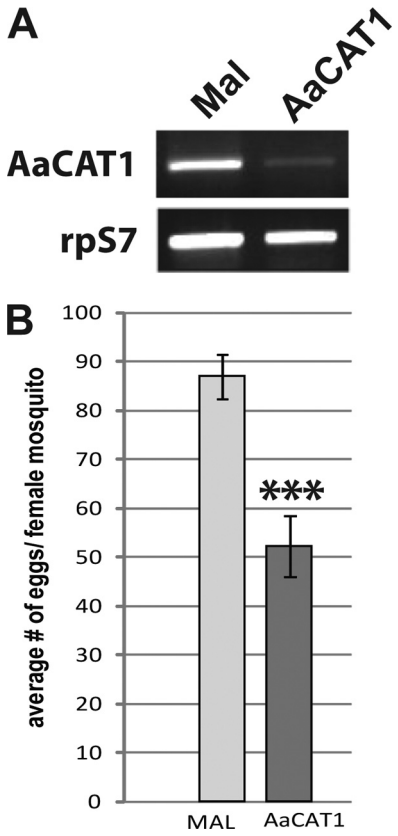

FIGURE 9. ***AaCAT1* knockdown affects mosquito fecundity.** *A*, RNAi-knockdown efficiency control. *AaCAT1* mRNA expression levels were determined via RT-PCR in control and RNAi-knockdown mosquitoes. *B*, effect of *AaCAT1* knockdown on egg numbers. dsRNA-injected mosquitoes were fed chicken blood. Fully engorged females were transferred in individual vials containing a wet cotton ball. Egg numbers were determined 96 h after the blood meal. Values are means ± S.E. (*error bars*) for 40 females. This experiment was repeated three times with similar results. Significance was determined using an unpaired Student's *t* test.

Until now, the functions of CATs in non-mammalian model systems were ambiguous and widely inferred based on the phylogenetic proximity of predicted protein sequences. Our phylogenetic analysis suggests that the CAT and HAT subfamily diverged from a common ancestor around 2.6 billion years ago. AaCAT1 and AaCAT3, together with *Drosophila* SLIF, form the most recent ~100 million-year-old expansion in the CAT subfamily, which is clearly separated from the mammalian and nematode CATs (Fig. 2). Therefore, the function of AaCAT1-like transporters cannot be inferred through phylogenetic proximity to the characterized vertebrate transporters and can only be determined by direct assay. This also raises the possibility that specific inhibitors to these transporters could be identified with little or no effect on the vertebrate counterparts.

We were able to express *AaCAT1* in a heterologous expression system suitable for comprehensive analysis of transport proteins. The results obtained from the analysis of *AaCAT1* expressed in *Xenopus* oocytes suggest that AaCAT1 acts as a histidine-selective transporter with relatively high affinity to L-His (Figs. 5–7). Therefore, its properties differ from the classical y^+ system that does not discriminate cationic amino acids and has even better capacity to transport arginine and lysine (29). In addition, AaCAT1 displays strong stereo-specificity

toward the L-enantiomer of its substrate (Fig. 5). With notably less substrate-induced current, it responds to L-ornithine but not to other tested metabolic amino acids. Among amino acid-derived neurotransmitters, only DA induces notable changes in AaCAT1-associated currents (Fig. 3); however, the functional significance of this interaction is not clear.

The estimated affinity of AaCAT1 for His was 5 times higher than the previously reported K_m of L-Arg transport by mouse CAT-1 (30) and is comparable with other reported K_m values for mammalian CAT1 and CAT2 interacting with their preferred substrates: arginine, lysine, and ornithine (29). However, L-histidine transport by these CATs was notably smaller (30) and was only detectable at low pH, where His is predominantly protonated (31). In our analysis, AaCAT1 generated large currents at neutral pH 7.2 (Figs. 3–5). The current-derived calculations of the affinity constant consider only the charged fraction of the substrate. The actual affinity of AaCAT to His^+ could be significantly higher (*e.g.* $E_{0.5}{}^{\text{L-His}^+} = 20.7 \pm 4\ \mu$M and $K_{0.5}{}^{\text{L-His}} = 27.5 \pm 10.37\ \mu$M (considering 6.1% protonated His^+ at pH 7.2). Hence, selective interaction with His^+ may cause interesting phenomena in the function of AaCAT1. First, it shifts this transport mechanism into a high affinity region, which is typically identified for transporters with narrow substrate specificity. Second, upon acidification of the extracellular medium, a significant amplification of substrate-mediated electrical or chemical signals might occur on the cell membrane of *AaCAT1*-expressing cells.

We attempted to analyze AaCAT1 function at alkaline conditions. Unexpectedly, we identified significant endogenous cationic amino acid-induced currents that interfere with AaCAT1 activity. Alkalinization to pH 8.2 enables quasiuniform Arg^+, Lys^+, and His^+ currents in both *AaCAT1* and control uninjected oocytes. Therefore, we cannot make any statements regarding the function of AaCAT1 in alkaline conditions.

It is possible that AaCAT1 acts as a transceptor involved in both transport and signaling processes. This would comprise a unique mechanism for signaling of changes in concentrations of essential L-His in the mosquito hemolymph, and such a signal could be amplified upon acidification. Additional studies on AaCAT1 function are necessary to test this interesting hypothesis.

The *AaCAT1* gene has a unique expression pattern (Fig. 8). mRNA is detectable during the fourth larval instar, but the AaCAT1 protein was not detected until the pupal and adult stages. These data suggest that AaCAT1 has no role in embryonic or postembryonic developmental processes and that its function is probably adult-specific. To our knowledge, this is the first report of an AA transporter with such restricted expression patterns; the closely related *Drosophila* SLC-7 transporter *slif* is strongly expressed in larval stages of fruit flies and plays a prominent role in the regulation of larval development (8). *AaCAT1* mRNA expression was detected in many organs/body parts with the exception of the head, with high relative expression levels in the flight muscle tissue of the thorax. The functional significance of this finding is unclear.

Injection of dsRNA into the hemocoel of adult mosquitoes has been shown to be an effective method to achieve strong RNAi-mediated gene knockdowns in a variety of different tissues (4, 6, 32, 33), and overall knockdown of *AaCAT1* was very strong after injection (Fig. 9*A*). Knockdown of *AaCAT1* resulted in a significant reduction in egg numbers (Fig. 9*B*), similar to reductions that have been observed as a result of the knockdown of other proteins of the fat body nutrient signaling cascade in mosquitoes (4, 5). However, the finding that *AaCAT1* knockdown mosquitoes are still able to produce a considerable number of viable eggs suggests that there are redundant AA signaling and transport systems that perform similar tasks as this protein.

In summary, we report the characterization of a mosquito CAT with strong substrate specificity to L-histidine as never before reported for a member of the SLC7-CAT subfamily. *AaCAT1* has a unique expression profile and is only found in pupae and adult mosquitoes. It is part of the AA signaling pathway and is involved in mosquito egg development.

Several facts make this transporter an interesting target for the development of novel, environmentally safe insecticides. First, it forms a distinct phylogenetic cluster with other insect CATs; second, its transport characteristics are very unlike vertebrate CATs (it specifically transports an essential AA); and third, it is part of the mosquito nutrient-sensing system and is associated with insect reproduction.

REFERENCES

1. Attardo, G. M., Hansen, I. A., and Raikhel, A. S. (2005) *Insect Biochem. Mol. Biol.* **35,** 661–675
2. Arrese, E. L., and Soulages, J. L. (2010) *Annu. Rev. Entomol.* **55,** 207–225
3. Baker, K. D., and Thummel, C. S. (2007) *Cell Metabolism* **6,** 257–266
4. Hansen, I. A., Attardo, G. M., Park, J. H., Peng, Q., and Raikhel, A. S. (2004) *Proc. Natl. Acad. Sci. U.S.A.* **101,** 10626–10631
5. Hansen, I. A., Attardo, G. M., Roy, S. G., and Raikhel, A. S. (2005) *J. Biol. Chem.* **280,** 20565–20572
6. Attardo, G. M., Hansen, I. A., Shiao, S. H., and Raikhel, A. S. (2006) *J. Exp. Biol.* **209,** 3071–3078
7. Verrey, F., Closs, E. I., Wagner, C. A., Palacin, M., Endou, H., and Kanai, Y. (2004) *Pflugers Arch.* **447,** 532–542
8. Colombani, J., Raisin, S., Pantalacci, S., Radimerski, T., Montagne, J., and Léopold, P. (2003) *Cell* **114,** 739–749
9. Hennig, K. M., Colombani, J., and Neufeld, T. P. (2006) *J. Cell Biol.* **173,** 963–974
10. Gutierrez, E., Wiggins, D., Fielding, B., and Gould, A. P. (2007) *Nature* **445,** 275–280
11. Goberdhan, D. C., Meredith, D., Boyd, C. A., and Wilson, C. (2005) *Development* **132,** 2365–2375
12. Martin, J. F., Hersperger, E., Simcox, A., and Shearn, A. (2000) *Mech. Dev.* **92,** 155–167
13. Hays, A. R., and Raikhel, A. S. (1990) *Dev. Genes Evol.* **199,** 114–121
14. Altschul, S. F., Madden, T. L., Schäffer, A. A., Zhang, J., Zhang, Z., Miller, W., and Lipman, D. J. (1997) *Nucleic Acids Res.* **25,** 3389–3402
15. Tamura, K., Dudley, J., Nei, M., and Kumar, S. (2007) *Mol. Biol. Evol.* **24,** 1596–1599
16. Edgar, R. C. (2004) *Nucleic Acids Res.* **32,** 1792–1797
17. Shaffer, P. L., Goehring, A., Shankaranarayanan, A., and Gouaux, E. (2009) *Science* **325,** 1010–1014
18. Zuckerkandl, E., and Pauling, L. (1965) in *Evolving Genes and Proteins* (Bryson, V., and Vogel, H. J., eds) pp. 97–166, Academic Press, Inc., New York
19. Chomczynski, P., and Sacchi, N. (1987) *Anal. Biochem.* **162,** 156–159
20. Boudko, D. Y., Kohn, A. B., Meleshkevitch, E. A., Dasher, M. K., Seron,

T. J., Stevens, B. R., and Harvey, W. R. (2005) *Proc. Natl. Acad. Sci. U.S.A.* **102,** 1360–1365
21. Meleshkevitch, E. A., Assis-Nascimento, P., Popova, L. B., Miller, M. M., Kohn, A. B., Phung, E. N., Mandal, A., Harvey, W. R., and Boudko, D. Y. (2006) *J. Exp. Biol.* **209,** 3183–3198
22. Miller, M. M., Popova, L. B., Meleshkevitch, E. A., Tran, P. V., and Boudko, D. Y. (2008) *Insect Biochem. Mol. Biol.* **38,** 923–931
23. Etoh, M., and Yoshii, K. (1994) *Comp. Biochem. Physiol. Physiol.* **109,** 361–367
24. Miller, A. J., Smith, S. J., and Theodoulou, F. L. (1994) *Symp. Soc. Exp. Biol.* **48,** 167–177
25. Bauch, C., and Verrey, F. (2002) *Am. J. Physiol. Renal Physiol.* **283,** F181–F189
26. Dissanayake, S. N., Ribeiro, J. M., Wang, M. H., Dunn, W. A., Yan, G., James, A. A., and Marinotti, O. (2010) *BMC Res. Notes* **3,** 248
27. Hediger, M. A., Romero, M. F., Peng, J. B., Rolfs, A., Takanaga, H., and Bruford, E. A. (2004) *Pflugers Arch.* **447,** 465–468
28. Closs, E. I., Boissel, J. P., Habermeier, A., and Rotmann, A. (2006) *J. Membr. Biol.* **213,** 67–77
29. Devés, R., and Boyd, C. A. (1998) *Physiol. Rev.* **78,** 487–545
30. Kim, J. W., Closs, E. I., Albritton, L. M., and Cunningham, J. M. (1991) *Nature* **352,** 725–728
31. Vékony, N., Wolf, S., Boissel, J. P., Gnauert, K., and Closs, E. I. (2001) *Biochemistry* **40,** 12387–12394
32. Biessmann, H., Andronopoulou, E., Biessmann, M. R., Douris, V., Dimitratos, S. D., Eliopoulos, E., Guerin, P. M., Iatrou, K., Justice, R. W., Kröber, T., Marinotti, O., Tsitoura, P., Woods, D. F., and Walter, M. F. (2010) *PLoS One* **5,** e9471
33. Drake, L. L., Boudko, D. Y., Marinotti, O., Carpenter, V. K., Dawe, A. L., and Hansen, I. A. (2010) *PLoS One* **5,** e15578
34. Saitou, N., and Nei, M. (1987) *Mol. Biol. Evol.* **4,** 406–425
35. Felsenstein, J. (1985) *Evolution* **39,** 783–791